THE ASTRONOMICAL JOURNAL VOLUME 114, NUMBER 2 AUGUST 1997

THE STELLAR CONTENT AND THE STAR FORMATION HISTORY OF THE LOCAL GROUP DWARF GALAXY LGS 3[1]

A. APARICIO[2]

Instituto de Astrofísica de Canarias, E-38200 La Laguna, Tenerife, Canary Islands, Spain
Electronic mail: aaj@iac.es

C. GALLART

Observatories of the Carnegie Institution of Washington, 813 Santa Barbara Street, Pasadena, California 91101
Electronic mail: carme@ociw.edu

G. BERTELLI

Dipartimento di Astronomia, Vicolo dell'Osservatorio 5, I35122 Padova, Italy
and Fellow of the Consiglio delle Ricerche (CNR-GNA), Roma, Italy
Electronic mail: bertelli@astrpd.pd.astro.it

Received 1997 March 13; revised 1997 April 29

ABSTRACT

The star formation history (SFH) and the properties of the dwarf galaxy LGS 3 are analyzed using color-magnitude (CM) diagrams plotted from *VRI* photometry of 736 stars. The distance to the galaxy is estimated through the position of the tip or the red giant branch. Two acceptable results have been obtained: 0.77 ± 0.07 Mpc and 0.96 ± 0.07 Mpc, although the first value is favored by complementary considerations on the stellar content of the galaxy. Both values make LGS 3 a possible satellite of M31 or of M33. The SFH is investigated for each of the two adopted distances comparing the observed (CM) diagrams with model CM diagrams computed for different star formation rates ($\psi(t)$) and chemical enrichment laws ($Z(t)$). The results are compatible with LGS 3 having been forming stars since an early epoch, 15–12 Gyr ago, at an almost constant rate if distance is 0.77 Mpc or at an exponentially decreasing rate if distance is 0.96 Mpc. According to our models, the current metallicity would range from $Z\simeq0.0007$ to $Z\simeq0.002$. Other results are the current $\psi(t)$: $(0.55\pm0.04)\times10^{-10}$ $M_\odot$ yr^{-1} pc^{-2} or $(0.47\pm0.07)\times10^{-10}$ $M_\odot$ yr^{-1} pc^{-2}, depending of the distance, and its average for the entire life of the galaxy, $\bar{\psi}=(1.4\pm0.1)\times10^{-10}$ $M_\odot$ yr^{-1} pc^{-2}. At the present $\psi(t)$, the probability of LGS 3 having an H II region is 0.2, which is compatible with the fact that no H II regions have been found in the galaxy. Its fraction of gas relative to the mass intervening in the chemical evolution is about 0.40 and its percentage of dark matter (that which cannot be explained as stellar remnants or by extrapolation of the used IMF to low masses) is 95%. The results for $\psi(t)$ and $Z(t)$ for $d=0.77$ Mpc are compatible with a moderate outflow of well mixed material ($\lambda=3$), but large outflow rate ($\lambda=30$) is required to account for the results for $d=0.96$ Mpc. The latter would imply that, if the amount of dark mass associated to the galaxy is constant, the initial dark matter fraction was about 50%. In both cases, a large fraction of freshly made metals ($\gamma=0.85$ for the case of $d=0.77$ Mpc and $\gamma=0.36$ for $d=0.96$ Mpc) should also escape from the galaxy before mixing with the interstellar medium to make the results compatible with the theoretical yields. LGS 3 is considered an intermediate type between dIr and dE. However we find that it shows characteristics typical of dIrs (the M_{gas}/L_B ratio and the SFH shape), the main difference being that its mass and star formation rate (present and averaged) are one to two orders of magnitude smaller than those of other dIrs. This makes the absence of H II regions a simple probabilistic effect. Considering this and the fact that LGS 3 can continue to form stars for a further 10 Gyr at a rate equal to that averaged for its past history, we conclude that this galaxy may be considered just a dIr in the tail of the distributions of mass, luminosity and star formation rate.
 [S0004-6256(97)01008-X]

[1]Based on observations made with the Nordic Optical Telescope operated on the island of La Palma in the Spanish Observatorio del Roque de los Muchachos of the Instituto de Astrofísica de Canarias.

[2]Presently at Observatories of the Carnegie Institution of Washington, 813 Santa Barbara St., Pasadena, CA 91101.

1. INTRODUCTION

Dwarfs seem to be the most abundant kind of galaxies in the Universe. That is at least the case for the Local Group, where all but four of its members are dwarfs. Although the light and the dynamics of the Local Group are dominated by the two largest galaxies, Andromeda and the Milky Way, the spatial distribution, velocities and other physical properties of dwarf galaxies in the Group and its neighborhood should provide information on its dynamical and evolutionary properties. In particular, the interconnections of the Milky Way with its satellites may contain clues for the mechanisms in which the galaxy was formed (see Majewski 1994). Dwarf galaxies could also play an important role in cosmological models, in particular, in relation to the issue of whether galaxies formed in a cold or in a hot dark matter scenario.

Dwarf galaxies can be divided into two large groups: dwarf ellipticals (dEs; we include the dwarf spheroidal galaxies in this group) and dwarf irregulars (dIrs). Both kinds of dwarfs cover similar ranges of mass and luminosity, the key difference between them being, besides morphology, that the latter have a much larger amount of gas and young stars than the former, where H II regions are absent. The $M_{\rm H\,I}/L_B$ ratio, which is of the order of 1 for dIrs and close to 0 for dEs, can be used to separate between both groups (Da Costa 1997). dEs and dIrs also show a decoupled spatial distribution in the Local Group: dEs are preferentially distributed close to the largest galaxies, while dIrs are found normally far away from these systems and many of them could be field galaxies rather than Local Group members. But the boundaries between dEs and dIrs are not sharp. Focusing on the stellar population, many dEs show indication of intermediate-age or even young stars (Smecker-Hane *et al.* 1996; Freedman 1994, and references therein), while most dIrs show the so-called Baade's sheet (Baade 1963) which would be composed by a large number of intermediate-age and old stars[3] if the generality of dIr have star formation histories (SFH) like those of NGC 6822 (Gallart *et al.* 1996b, 1996c) and Pegasus (Aparicio *et al.* 1997). A gradation exists in the properties from dEs to dIrs and it is argued that LGS 3 may be a transition object between a dIr galaxy and a dE (see below).

LGS 3 was discovered by Karachentseva (1976). Thuan & Martin (1979) measured its H I content obtaining a negative velocity -280 ± 8 km s^{-1} or, relative to the centroid of the Local Group (LG), -0.41 ± 8 km s^{-1} and an H I mass of $M_{\rm H\,I}=(2.15\pm0.36)\times10^5$ M$_\odot$, assuming the galaxy being at the same distance as M33 (0.817 Mpc was used). Tifft & Cocke (1988) obtained new measures of H I and a velocity relative to the Sun of -286 km s^{-1}. Lo *et al.* (1993) estimated the H I mass of LGS to be $(4.0\pm0.5)\times10^5$ M$_\odot$ Mpc^{-2} and its total mass $(1.8\pm1)\times10^7$ M$_\odot$, for which they adopted a distance of 0.76 Mpc. Early optical studies of the galaxy are those by Schild (1980), who obtained a value for its total magnitude and by Christian & Tully (1983), who performed photometry of individual stars and obtained a first independent estimate of the distance between 0.7 and 1.2 Mpc. Late studies of LGS 3 are those by Lee (1995), Tikhonov & Makarova (1996), Mould (1997), and Karachentseva *et al.* (1996). Lee has estimated the metallicity of the galaxy to be [Fe/H] $=-2.10\pm0.22$ and the distance, 0.81 ± 0.08 Mpc from the width and position of the red giant branch (RGB) and the tip of the RGB (TRGB). In turn, Tikhonov & Makarova have estimated a distance of 0.6 ± 0.1 Mpc using the TRGB and the magnitude of the brightest stars in the galaxy. Mould also uses the TRGB to estimate a distance of 0.81 ± 0.15. Finally, Karachentseva *et al.* have obtained a total apparent magnitude of $B_T=16.18$ and an axial ratio of 0.67.

Much effort has been devoted to the determination of the properties of LGS 3. The distance estimates indicate that it might be a satellite of M33. But the main interest of this object comes from the fact that, as mentioned above, it may be a transition object between a dIr galaxy and a low-luminosity dE (see Gallagher & Wyse 1994), having properties typical of both. If dwarf galaxies evolve from star forming to passive objects, LGS 3, together with other systems, like Phoenix (van de Rydt *et al.* 1991), could be in a transition stage. LGS 3 shows a CM diagram similar to those of dE galaxies although with a small number of blue stars. It also has a small but significant amount of gas. Apparently, it is not currently forming stars or, at least, its present star formation rate (SFR) is very low, since the galaxy shows no traces of ionized gas. Its role as a possible missing link between the two subtypes of dwarf galaxies make a deep understanding of the properties of LGS 3 very important. Knowledge of its star formation history (SFH) will certainly help to reach that understanding. In this paper, we discuss what the SFH of LGS 3 may have been, using new ground-based photometry of its stars.

In Sec. 2 the observations are presented. Section 3 discusses the CM diagrams. In Sec. 4 the distance is derived. Section 5 deals with the derivation of the SFH and Sec. 6 is devoted to the discussion of the resulting SFH. In Sec. 7 the chemical scenarios that would be compatible with the found SFH are investigated. In Sec. 8 integrated properties of the galaxy are discussed. In Sec. 9 the main conclusions of the work are summarized.

2. OBSERVATIONS AND DATA REDUCTION

LGS 3 was observed in V, R, and I (Johnson-Cousins) in 1993 October, at the Cassegrain focus of the Nordic Optical Telescope (NOT), at Roque de los Muchachos Observatory on the island of La Palma. The reader is referred to the paper by Aparicio & Gallart (1995) where details about this observing run are given. We give here a short description of the observations and data reduction. A thick, blue coated, Thomson CCD of 1024×1024 pixels was used. It provided a pixel size of 0.14″ and a total field of $143\times143(″)^2$. This field covered most of the galaxy optical body, although not completely. Total integration times were 6000 s in V, 3200 s in R, and 4600 s in I. Several frames were taken in each band, moving the telescope slightly (about 3 to 5 arcsec) between each two exposures, in order to reduce systematic pixel-to-

[3]In this paper, we mean by old stars those older than 10 Gyr, by intermediate-age stars those with ages between 1 and 10 Gyr and by young stars those younger than 1 Gyr.

TABLE 1. Journal of observations (1993 October 17).

Time(UT)	Object	Filter	Exp. time (s)	FWHM (″)
02:32	LGS 3	I	900	0.64
02:50	LGS 3	I	900	0.66
03:09	LGS 3	R	900	0.69
03:24	LGS 3	R	700	0.74
03:43	LGS 3	V	1000	0.74
04:18	Field	R	600	0.84
04:32	Field	I	700	0.94
00:54	LGS 3	V	1000	0.78
01:12	LGS 3	I	900	0.61
01:29	LGS 3	I	900	0.73
01:46	LGS 3	R	800	0.78
02:00	LGS 3	R	800	0.74
02:43	LGS 3	V	1000	0.74
03:00	LGS 3	V	1000	0.70
03:21	LGS 3	V	1000	0.78
03:40	LGS 3	V	1000	0.75
03:59	LGS 3	I	1000	0.70

pixel and position-dependent effects on the stellar magnitudes. The journal of observations is given in Table 1. The UT for the beginning of each exposure are given in column 1 all of them corresponding to 1993 October 17; column 2 lists the target (LGS 3 or a companion field); column 3 gives the filter; column 4 lists the integration times; and the full width at half maximum (FWHM) of the stellar profiles is given in column 5.

The CCDRED package of IRAF was used to pre-process the data, using bias, dark and flatfield frames obtained during the observing nights. The effect of the dispersed light produced by the LED used to recognize the position of the filter wheel was also satisfactorily corrected (see Aparicio & Gallart 1993 and 1995). DAOPHOT II and ALLSTAR (Stetson 1993) was used to derive the magnitudes of the stars, through multiple fitting of a point spread function (PSF) to the stellar profiles. An empirical PSF, varying with position on the frame, was obtained for each image. A Moffat analytical function and a table of residuals were computed, both obtained from a large number of well-shaped stars in each frame. The residuals of the fit, σ, and the CHI and SHARP parameters of ALLSTAR were used to select the stars with *good* photometry. Only stars with $\sigma<0.15$, CHI<1.2 and $-1.2<$SHARP<1.2 in all the frames (V, R, and I) were retained. All in all, 736 stars were kept, measured in at least two colors. Figure 1 shows the plot of σ values given by ALLSTAR for the retained stars. These plots are interesting because the σ values are representative of the internal errors of the photometry as a function of magnitude: following Stetson & Harris (1988), the internal errors, defined as the σ values obtained from frame-to-frame agreement, would not differ by more than about 20% from the σ values provided by ALLSTAR.

Aperture corrections were obtained using the image's FWHM and the relation given by Aparicio & Gallart (1995), which are valid for the observing run under discussion:

$$m_{\rm psf}-m_{\rm ap}=-0.346+1.336\rm FWHM,$$

where $m_{\rm psf}$ are magnitudes from PSF fitting and $m_{\rm ap}$ are aperture magnitudes. The $m_{\rm ap}$ were corrected for atmospheric

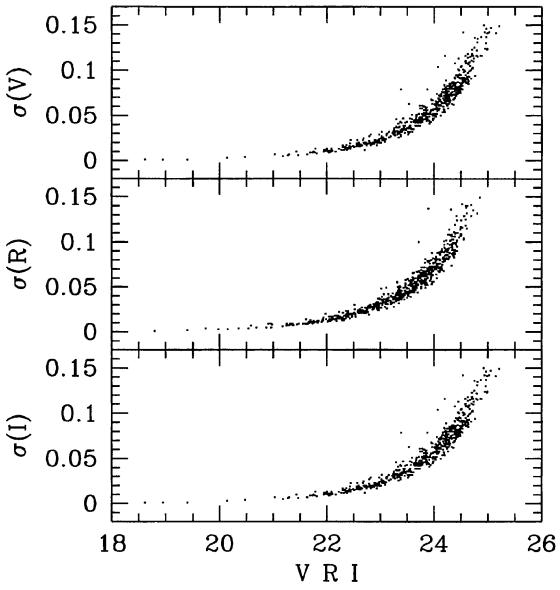

FIG. 1. Residuals of the fitting of the PSF models vs magnitude, as provided by ALLSTAR, for the stars included in the final photometric list of LGS 3.

extinction and then transformed into the Johnson-Cousins standard system, using the relations given in Aparicio & Gallart (1995):

$$(V-v)=23.707-0.010(V-R),$$

$$(R-r)=24.344-0.021(V-R),$$

$$(I-i)=23.746+0.010(V-I),$$

where capital letters refer to Johnson-Cousins magnitudes and lower-case letters stand for $m_{\rm ap}$ magnitudes above the atmosphere. These transformation equations, as well as the atmospheric extinctions in each band and each night, were obtained from twenty-three measurements in each band of a total of 18 stars from the list of Landolt (1992). The photometric conditions were particularly good, producing very small zero-point errors: 0.004 for V, 0.005 for R and 0.009 for I. The main zero-point error source is therefore the $m_{\rm psf}-m_{\rm ap}$ correction. Taking all the error sources into account, we may estimate that our photometrical calibration is affected by total zero-point errors of about 0.01 to 0.02 in the three bands. The full photometric list will be made available by the authors on request. Figure 2 shows the I image.

We have compared our photometry with the *VRI* photometry of Lee (1995) and the *VI* photometry of Mould (1997). No color terms are apparent but the following systematic zero points have been found:

$$V_{\rm Lee}-V_{\rm here}=-0.09\pm0.01,$$

$$R_{\rm Lee}-R_{\rm here}=+0.03\pm0.02,$$

$$I_{\rm Lee}-I_{\rm here}=-0.02\pm0.02,$$

$$V_{\rm Mould}-V_{\rm here}=+0.17\pm0.01,$$

$$I_{\rm Mould}-I_{\rm here}=+0.24\pm0.01.$$

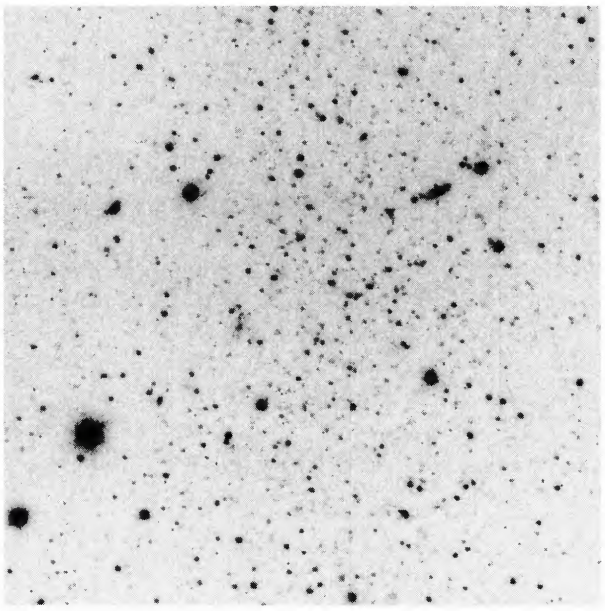

FIG. 2. I image of LGS 3. The total field is 143×143 $(")^2$ and the integration time 4600 s. North is *up*, east is *left*.

About 25 stars with $V<22.5$ have been used in each case. Standard errors are quoted.

3. THE COLOR-MAGNITUDE DIAGRAM

Figures 3 and 4 show the I vs $(V-I)$ and V vs $(V-R)$ CM diagrams of LGS 3. Contamination by foreground stars is very small for LGS 3, but may produce non-negligible effects on the star counts of the brightest, less populated parts of the CM diagram. To check this point, two additional frames of a field adjacent to LGS 3 were taken in R and I during the same observing run. Exposing times were 600 and 700 s, respectively (see Table 1). Only eleven stars have been resolved in the field. Colors and magnitudes of ten of these stars are smoothly distributed in the range $17<I<22.0$, $0.0<(R-I)<0.9$. The remaining star is a redder, fainter one and its photometry might be affected by a large random effect. This information will be used later on to correct the star counts in the CM diagrams. Since the integration times are short in the field frames, completeness might be significantly smaller than 1 at $I\simeq22.0$. But the number of foreground stars is so small that this cannot introduce any appreciable effect on the star counts in the lower part of the LGS 3 CM diagram.

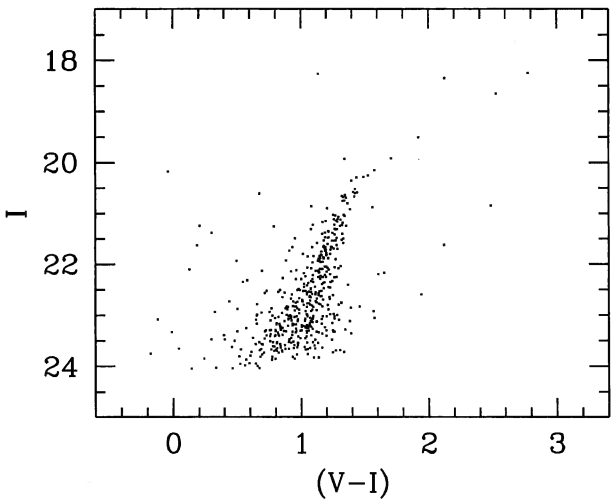

FIG. 3. Observational I vs $(V-I)$ CM diagram of LGS 3.

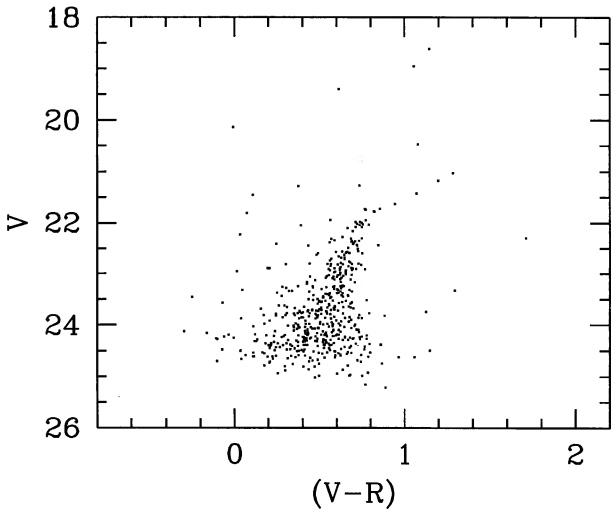

FIG. 4. Observational V vs $(V-R)$ CM diagram of LGS 3.

The main feature of the LGS 3 CM diagrams is the clump that extends from $(V-R)\simeq0.2$, $(V-I)\simeq0.7$ at the faint magnitude limit, to $[(V-R),V]\simeq[0.8,22.0]$ and $[(V-I),I]\simeq[1.5,20.5]$. This feature is what we have been calling the *red-tangle* in previous papers (see Aparicio & Gallart 1994). In principle, it is composed of the RGB and the asymptotic giant branch (AGB) locus of old and intermediate-age stars and by intermediate-age blue loops. The fact that the red-tangle is so narrow necessarily implies a small range of metallicities of the stars of LGS 3, although their ages may be in a large interval. We will discuss this in detail below in Secs. 5 and 6.

For moderately high metallicities, of the order of a few thousands in Z, the AGB stars produce what we call the *red-tail* (Aparicio & Gallart 1994). Its redward extension may be an indication of the metallicity of the system. Again LGS 3 has too few stars for the redward extension to be clearly determined. The very bright stars at $I\simeq18.5$, $(V-I)\simeq2.6-2.8$ could be AGBs but they may also be foreground stars and AGBs would extend just up to $(V-I)\simeq2.0$.

Young stars would be found in the main sequence (MS), the blue-loops or the red supergiant (RSG) phases. The few stars bluer than $(V-I)\simeq0.6$ may be in one of the first two evolutionary phases (our companion field has some 2 stars in this area). The star at $I\simeq18.0$, $(V-I)\simeq1.2$ could be a RSG but, it could also be a foreground star.

4. THE DISTANCE

The TRGB is the point of the CM diagram at which low-mass stars undergo the He-flash. The bolometric luminosity

of this point is almost constant for different ages and moderate metallicities and therefore, it is an important distance estimator (Lee *et al.* 1993). It is most valuable in galaxies like LGS 3, which have a low probability of having even a single Cepheid star. Unfortunately, the upper part of the RGB locus of LGS 3 is split into several small clumps in such a way that it is quite difficult to decide which of them actually marks the TRGB. Application of a Sobel filter $[-1,0,+1]$ to the luminosity function, after adequate smoothing, results in two clearly separated peaks close to the upper part of the RGB, at magnitudes $I_{\rm TRGB}=20.52\pm0.08$ and $I_{\rm TRGB}=21.04\pm0.05$. The first value seems more stable and corresponds to the upper cut-off of the RGB (see Fig. 3). Errors are simple estimates of the wideness of the peaks at 1/3 of their maxima. Lee (1995) found the TRGB of LGS 3 at $I=20.4$, and Mould (1997) found it at $I=20.5\pm0.4$. These values are close to our first possibility, although some traces of the discontinuity at $I\simeq21.0$ can also be seen in Lee's and Mould's CM diagrams. Since the signal-to-noise ratio of our photometry at $I\sim21$ is quite good and we have no strong criterion to decide, we will use both values for the magnitude of the TRGB ($I=20.52$ and $I=21.04$) and analyze the resulting properties of the galaxy in both cases. The stars over the TRGB are mainly AGB stars. This means that the use of either value for the magnitude of the TRGB can in principle significantly affect the results for the SFH, since many more AGBs would be present if $I_{\rm TRGB}=21.04$.

To derive the distance modulus from the TRGB, the foreground extinction is needed. It can be estimated from Burstein & Heiles (1984) to be $A_B=0.16$, $A_V=0.12$, $A_R=0.09$, $A_I=0.07$. Using these values, the two possible de-reddened positions of the TRGB are $[(V-I)_0,I_0]_{\rm TRGB}=[1.33,20.45]$ and $[(V-I)_0,I_0]_{\rm TRGB}=[1.25,20.97]$. The distance modulus can now be calculated from the bolometric magnitude of the TRGB and an estimate of the metallicity. The latter can be obtained from the value of $(V-I)_0$ at $M_{I_0}=-3.5$ (~0.5 mag below the TRGB) using the relation given by Lee *et al.* (1993). The bolometric magnitude of the TRGB is then obtained as $M_{\rm bol}=-0.19[{\rm Fe/H}]-3.81$, which is transformed to the magnitude in the I band using $M_I=M_{\rm bol}-{\rm BC}_I$, where ${\rm BC}_I$ is the corresponding bolometric correction derived from ${\rm BC}_I=0.881-0.243(V-I)_{\rm TRGB}$ (Da Costa & Armandroff 1990). The resulting values of the distance modulus for each assumption of the TRGB are $(m-M)_0=24.43$ and $(m-M)_0=24.91$. The main error source is the uncertainty in $I_{\rm TRGB}$. Combined with the uncertainty in the extinction and in the calibration of the photometry, an estimate for the error of each of the former distance moduli is ±0.2 mag. Taking this into account, the two values for the distance are $d=0.77\pm0.07$ Mpc and $d=0.96\pm0.07$ Mpc. In summary, we can only say that the distance to LGS 3 is compressed between 0.7 and 1.0 Mpc. We will see later, from the results of the analysis of the SFH, that value $d=0.77\pm0.07$ Mpc seems more likely. These intervals can be compared with the values previously obtained by Mould (1997): 0.81 ± 0.15 Mpc, and by Lee (1995): 0.81 ± 0.08 Mpc, both from the TRGB and using the same method as here; by Tikhonov & Makarova (1996) from the TRGB and luminosities of the brightest stars: 0.6 ± 0.1 Mpc; and by Christian & Tully (1983) from the brightest RSG: $0.7-1.2$ Mpc.

5. DERIVATION OF THE STAR FORMATION HISTORY

It may be said at first glance that the stellar population of LGS 3 would be composed by a number of old and intermediate-age stars, populating the red-tangle structure, plus a small amount of young stars, populating the bluest part of the CM diagram. The absence of a well developed red-tail can be interpreted as either the stars' metallicity always being very low or as the small number of stars resulting in a very low probability of having stars in the AGB phase. The amount of information in the LGS 3 CM diagram is less than in the cases of Pegasus (Aparicio & Gallart 1995; Aparicio *et al.* 1997) or NGC 6822 (Gallart *et al.* 1996a, 1996b, 1996c) but several things can still be inferred about its SFH from the analysis that follows.

For the purposes of this paper, we consider the SFH to be a function of time accounting for all the characteristics which determine the formation of stars, mainly the star formation rate (SFR), the chemical enrichment law (CEL), and the initial mass function (IMF). Here we assume the IMF to be fixed. We use the Kroupa *et al.* (1993) function. Hence the SFR, which we will designate by $\psi(t)$ and the CEL, which we will designate $Z(t)$, both depending on time, are the functions we will use to characterize the SFH.

We have studied the SFH of LGS 3 via the comparison of its CM diagrams with model CM diagrams computed in a similar way as described in Gallart *et al.* (1996b, 1996c) and Aparicio *et al.* (1997). Model CM diagrams are synthetic CM diagrams in which observational effects have been simulated. For this, the procedure explained in detail in Aparicio & Gallart (1995) and Gallart *et al.* (1996b) has been followed. In the case of LGS 3, 8000 artificial stars have been used to determine the observational effects. The V, R, and I magnitudes of each star were simulated and they were added to the V, R and I images in groups of 40 stars at a time. DAOPHOT II and ALLSTAR were run for each of the the 600 resulting frames to recover the magnitudes of the artificial stars. These recovered magnitudes, together with their input values are the information necessary to build up the *crowding trial table* (see Aparicio & Gallart 1995) used to simulate the observational effects in the model CM diagrams. Observational effects are, in particular, incompleteness effects, systematic shifts in color and magnitude as well as internal and external errors, all them functions of stellar colors and magnitudes.

To analyze the SFH of LGS 3 with model CM diagrams, we have followed a different approach from that used for NGC 6822 (Gallart *et al.* 1996b, 1996c) and Pegasus (Aparicio *et al.* 1997). We have first generated a small number of model CM diagrams produced by $\psi(t)$ functions defined as

$$\psi(t)=const., \quad t_1\leq t<t_2,$$

$$\psi(t)=0, \quad t<t_1; t\geq t_2,$$

and with metallicities randomly distributed in a given interval $Z_1\leq Z(t)<Z_2$. t_1, t_2, Z_1 and Z_2 are the inputs changing from model to model. In other words, these CM diagrams

contain stars with ages and metallicities distributed in short intervals. We will term these as *partial models* and denote their $\psi(t)$ functions by ψ_i. They will later be combined to produce what we will term *global models*, used to search the best representation of the observed CM diagram. We have first chosen the age intervals (t_1 and t_2) for each partial model. They are from 15 to 12 Gyr, 12–9 Gyr, 9–6 Gyr, 6–3 Gyr, 3–1 Gyr, and 1–0 Gyr (in practice the star formation is stopped at $t=0.01$ Gyr which is the minimum age available in the stellar evolution library used, see Bertelli *et al.* 1994).

The color index and width of the red-tangle is related firstly to the mean metallicity and the metallicity dispersion of the stars and secondly with the age distribution. We have used this information to determine what the metallicity range (Z_1 and Z_2) should be that, given the age interval of each partial model, adequately reproduces both the position and width of the observed red-tangle. This has been done for all the age intervals except for the 1–0 Gyr one, for which most of the evolved stars are not in the red-tangle. The metallicity for this interval has been obtained extrapolating the metallicity law derived using the remaining intervals.

This approach to choose the metallicity law warrants a few comments. First, the reason we have adopted it is that we have no alternative information about $Z(t)$, lacking in particular measurements from H II regions or estimates from the structure of an AGB red-tail. Note furthermore that, in general, we use information of two kinds for studying the SFH: (i) position and overall shape of main structures in the CM diagram and (ii) distribution of stars inside and outside those structures (see Gallart *et al.* 1996b and Aparicio *et al.* 1997). Here, we are using information of the first kind to choose a valid $Z(t)$ law as the starting point. We no longer care about it in the rest of the process, in which we will use information of the second kind to put limits on $\psi(t)$ (see below). This strategy has the advantage of greatly reducing the number of partial models to be calculated, eliminating from the beginning all models which would produce a red-tangle with different width or in a different place from the observed one. It can be argued, however, that assuming that the entire width of the red-tangle is due to the metallicity dispersion will result in obtaining a SFH with a smaller dispersion in age. This is obviously true, but we prefer to adopt this position rather than the opposite, that would be to assume that stars at a given age do not have any metallicity dispersion, which would favor a larger age dispersion. If LGS 3 were an intermediate case between a dIr and a dE, we might expect it to show an age dispersion smaller than that of a dIr. By assuming that the entire width of the red tangle is due to the metallicity dispersion, we are favoring to find a small age dispersion. If, in spite of this fact, we still find a likely large age dispersion, we are in a better position to believe that such is really the case.

In summary, with the adopted procedure, we reduce the number of partial model CM diagrams to be computed to only 6 for each of the two possible distances. Figure 5 shows the $Z(t)$ laws corresponding to these distances. $Z(t)$ functions significantly different from these would produce model CM diagrams that do not match the observed one. Note that the only thing assumed at this level is that, if LGS 3 has stars

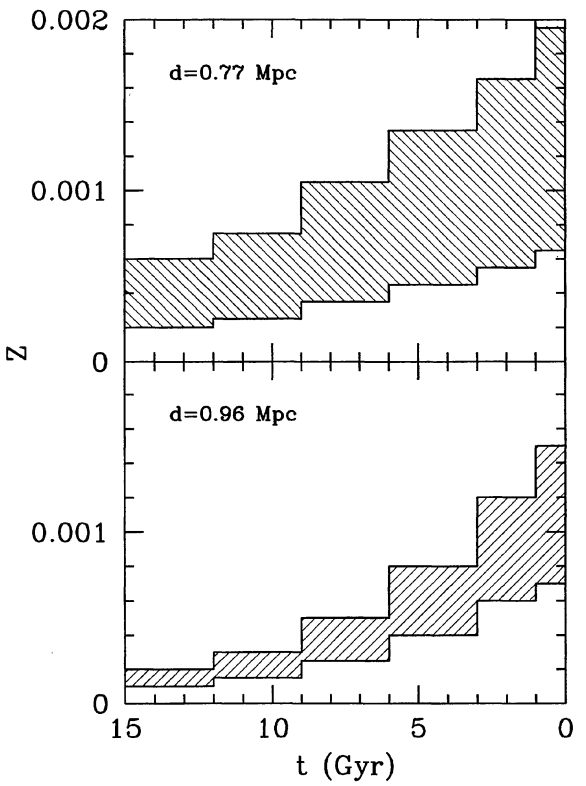

FIG. 5. The adopted metallicity laws for each of the two possible distances. Upper panel shows the region of the metallicities allowed for the case of distance $d=0.77$ Mpc. Stars of a given age in the models have their metallicities compressed in this region. Lower panel shows the same for the case $d=0.96$ Mpc. Laws which significantly differ from these would produce model CM diagrams not matching the observed one.

in a given age interval, their metallicities should be in the corresponding range shown in Fig. 5.

The comparison between model and observed CM diagrams intended to put limits on $\psi(t)$ is done through star counts in the eight regions of the CM diagrams defined in Fig. 6. These regions have been chosen to sample specific stellar evolutionary phases. Region 1 includes MS and blue-loop stars. Region 2 would be populated by RSGs and by bright AGBs. Regions 3 and 4 correspond to the part of the diagram where intermediate-age and old AGBs are expected to appear if the metallicity is not very low. Region 5 is defined just over the TRGB and would contain low-metallicity AGB stars. Regions 6, 7, and 8 sample the red-tangle. Figure 6 corresponds to $d=0.77$ Mpc. Regions are defined at the same positions in $[(V-I)_0, M_I]$ for $d=0.96$ Mpc. In this case, region 8 is not considered because its lower boundary is too close to the limit of the photometry.

The numbers of stars in each of the former regions of the observed I vs $(V-I)$ CM diagram are shown in Fig. 7 (solid lines) for both distances. These numbers have been corrected from foreground contamination using the information given in Table 2. This table contains the number identifying each region in the first column. The second column gives the adopted numbers of foreground stars contaminating each region. They have been determined from the photometry per-

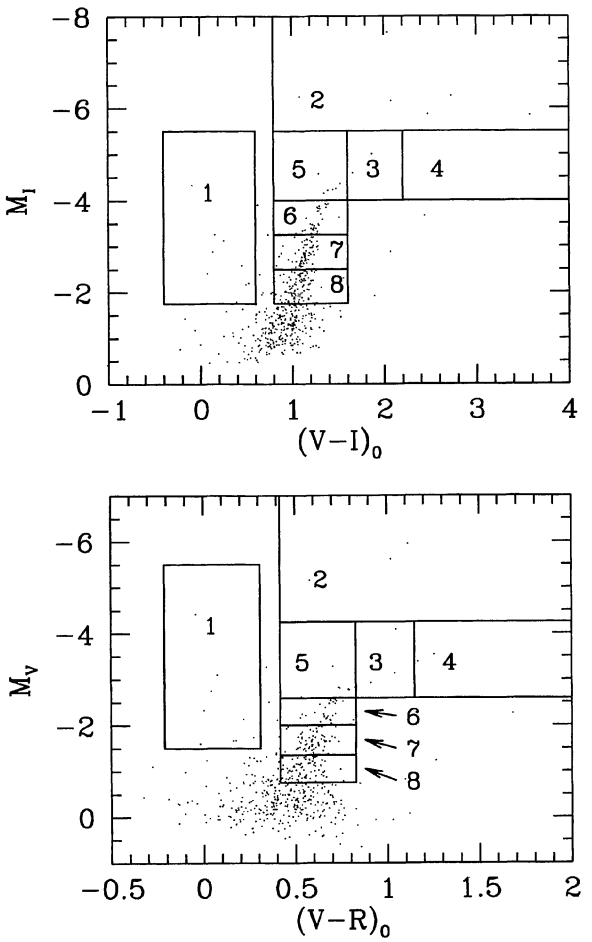

FIG. 6. The 8 regions used for the determination of $\psi(t)$ superimposed on LGS 3's M_I vs $(V-I)_0$ and M_V vs $(V-R)_0$ CM diagrams corrected for reddening and for a distance modulus of $(m-M)_0=24.43$ ($d=0.77$ Mpc).

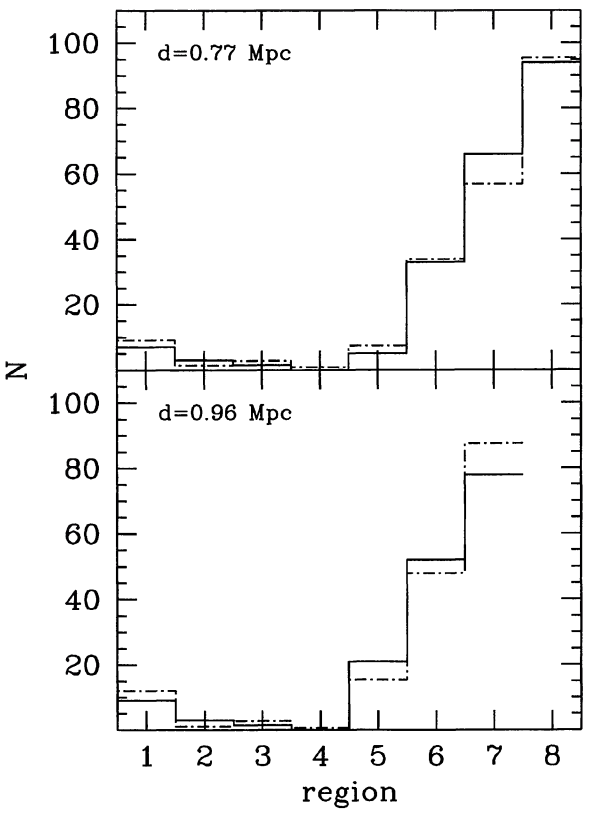

FIG. 7. Number of stars in each region of the I vs $(V-I)$ CM diagram for the two distances considered. Full lines refer to the observed diagram. Dashed lines correspond to the averages of all the accepted models.

formed in the comparison field (see Sec. 2). The numbers of foreground stars are very small, but can be relevant in the less populated regions. A single star appears in the foreground comparison field around the lower limit used to define region 3. This star is outside the region, but could be inside if the error intervals for the distance and the photometry are considered. For this reason, the value 0.5 has been adopted for the foreground stars in region 3.

Global models are obtained as a combination of partial models. They have arbitrary $\psi(t)$ functions produced by choosing the adequate fraction of stars of each partial model. Global models are those to be compared with the observed CM diagram to search for the SFH. But the global models do not need to be explicitly computed. Once the amount of stars with which each partial model populates each of the regions defined in the CM diagram is known, the amount of stars that populate the same regions for a given global model can be directly found as a linear combination of the form

$$N_{g,j}=\sum_{i=1}^{m} a_i k_i N_{i,j},$$

where $N_{g,j}$ is the number of stars in region j for the global model; $N_{i,j}$ is the same number corresponding to partial model i; k_i normalize each partial model to the same constant $\psi(t)$; a_i are the coefficients defining the global model and m is the number of partial models used (six in our case). In other words, the $N_{g,j}$ values are all we need for comparing the global models with observations. An arbitrarily large number of global models can be made by just changing a_i.

In practice, we have done the following. First, we have chosen for a_i the values 0, 0.5, 1, 1.5, 2, 3, 5, 8, 12, and 18 and we have computed all the $N_{g,j}$ corresponding to the one million possible global models resulting from giving to a_i all the possible variations of the former values. The $N_{g,j}$ are then normalized to reproduce the total number of stars in the observed CM diagrams inside the regions used:

TABLE 2. Adopted number of foreground stars.

CM region	Foreground
1	2
2	3
3	0.5
4	0
5	1
6	1
7	1
8	1

$$l\sum_{j=1}^{r} N_{g,j}=\sum_{j=1}^{r} N_{o,j},$$

where r is the total number of regions (seven or eight in our case) and $N_{o,j}$ is the number of stars in region j in the observed diagram. The absolute scale of $\psi(t)$ is set by this normalization; the particular values given to a_i mean only relative weights of the SFR at each epoch.

The SFR corresponding to each global model is then

$$\psi(t)=l\sum_{i=1}^{m} a_i k_i \psi_i,$$

where ψ_i corresponds to partial model i.

An error can be associated to each of $N_{g,j}$ and $N_{o,j}$ assuming Poissonian distributions of data. For the observed values the errors are simply

$$\sigma_{o,j}=N_{o,j}^{1/2}.$$

Errors of models have to include the different normalizations. First, the errors of partial models are

$$\sigma_{i,j}=k_i N_{i,j}^{1/2}.$$

Errors of global models are

$$\sigma_{g,j}=l\left(\sum_{i=1}^{m} a_i^2\sigma_{i,j}^2\right)^{1/2}.$$

Then, global models producing stars counts in each of the r regions of the two CM diagrams [I vs $(V-I)$ and V vs $(V-R)$] differing from the star counts of the observed CM diagrams by less than a given number of σ are selected; i.e., the models verifying

$$\delta_j \leqslant n\sigma_j \quad \forall j,$$

where $\delta_j=\mathrm{abs}(N_{g,j}-N_{o,j})$, $\sigma_j=(\sigma_{g,j}^2+\sigma_{o,j}^2)^{1/2}$ and n is the allowed error interval, expressed in σ.

6. THE RESULTING STAR FORMATION HISTORY

We have performed the former procedure for the two choices of the distance. There is no global model compatible with observations at the 1σ level; i.e., there is no global model which reproduces the number of stars in each of the r (seven or eight) regions of both CM diagrams to better than 1σ. 2.5% of global models are compatible with observations at the 1.33σ level for $d=0.77$ Mpc but models up to 2σ have to be accepted to have a similar amount in the case of $d=0.96$ Mpc. No models are compatible with observations at 1.33σ for this distance.

The SFH of any global model selected in this way would produce a CM diagram compatible with observations at the quoted level. A general representation can be provided by the average of all the selected models. Figure 8 shows the average $\psi(t)$ functions of models accepted at 1.33σ for distance $d=0.77$ Mpc and 2σ for distance $d=0.96$. Error bars show the dispersion of $\psi(t)$ for each age interval. In Fig. 7, the number of stars in the eight regions used in the observed I vs $(V-I)$ diagrams are compared with those produced by the averaged models. Similar representations are obtained for

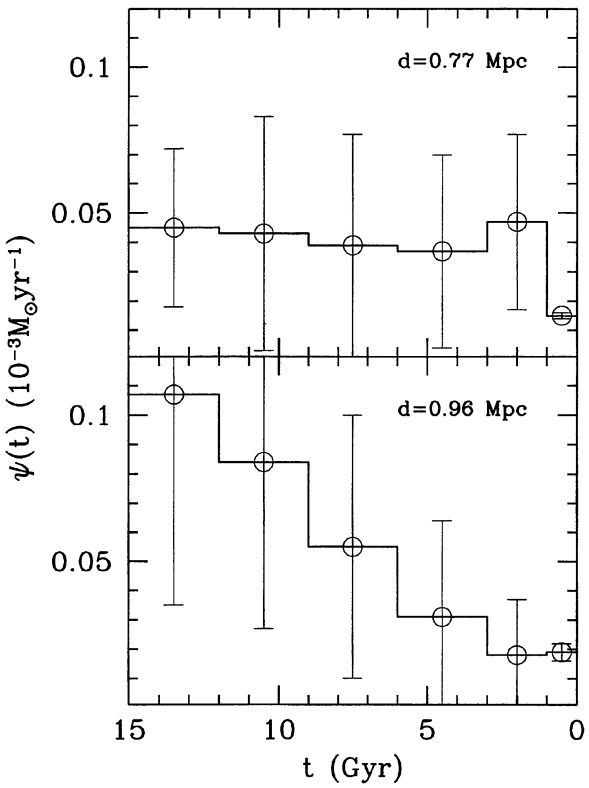

FIG. 8. Average of accepted $\psi(t)$ of LGS 3. Upper panel corresponds to $d=0.77$ Mpc and has been obtained averaging all models compatible with the corresponding observed CM diagrams at 1.33σ level. Lower panel corresponds to $d=0.96$ Mpc and has been obtained by averaging all models compatible with the corresponding observed diagrams at the 2σ level.

the V vs $(V-R)$ diagrams. The fact that results are worse for $d=0.96$ Mpc might be an indication that the right distance is 0.77 Mpc and that, therefore, the discontinuity in the RGB at $I\sim 21.00$ is a random effect. This distance agrees with the values found by Mould (1997) and Lee (1995), but it must be checked by another independent procedure.

Figure 8 shows that an almost constant (for $d=0.77$ Mpc) or decreasing (for $d=0.96$ Mpc) $\psi(t)$ can reproduce the observed CM diagrams. But the large error bars indicate that, for $t>1$ Gyr, $\psi(t)$ can vary within very wide intervals. However, $\psi(t)$ cannot move inside the error intervals in an arbitrary way. Figure 9 gives complementary information for the case of $d=0.77$ Mpc. To plot panel (a), the accepted global models have been divided into three sets, according to their $\psi(t)$ for the time interval 15 to 12 Gyr: those having $\psi(t)$ larger than 0.5σ over the average value; those having $\psi(t)$ closer than 0.5σ to the average and those having $\psi(t)$ smaller than 0.5σ below the average value. In other words, they have divided into models with high, intermediate and low $\psi(t)$ during the 3 first Gyrs. The same criterion has been applied to plot the rest of the panels, but using the value of $\psi(t)$ in different time intervals: panel (b) from 12 to 9 Gyr; panel (c) 9–6 Gyr; panel (d) 6–3 Gyr; panel (e) 3–1 Gyr. No division has been done for the interval from 1 to 0 Gyr because the value of $\psi(t)$ is very stable for this last period. The integrated $\psi(t)$ must account for the total number of stars in

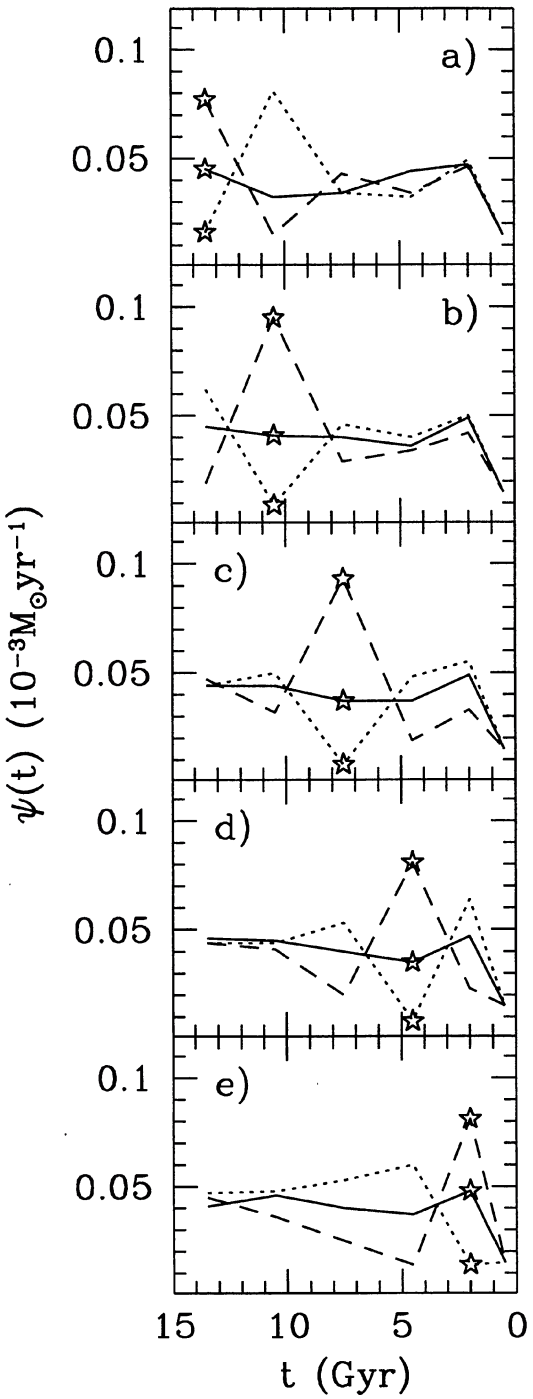

FIG. 9. Average of possible $\psi(t)$ functions considering several subsets according to the value of $\psi(t)$ (high, medium or low) at each of five time intervals. In each panel, dashed, full and dotted lines, respectively, correspond to averages of models having high, medium, and low $\psi(t)$ at the time interval marked by stars (see text for details).

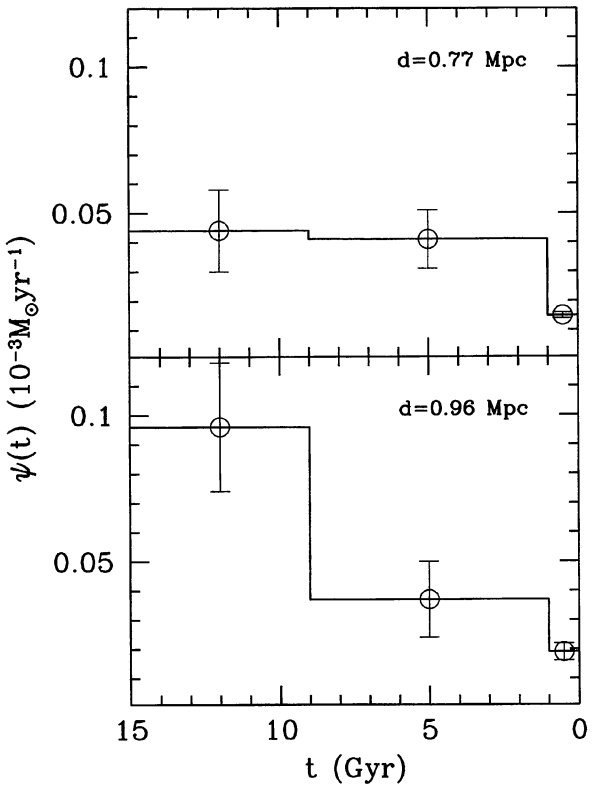

FIG. 10. Likely SFR of LGS 3 as a function of time, obtained from the same data plotted in Fig. 8 after rebinning time intervals. Upper panel corresponds to $d=0.77$ Mpc. Lower panel corresponds to $d=0.96$ Mpc.

the observed CM diagram. Therefore, if $\psi(t)$ is higher in a given time interval, it must be compensated for by lower $\psi(t)$ in other time intervals. This can be seen in Fig. 9. The interesting point is that the effects of choosing a higher or lower $\psi(t)$ in a given time interval are mostly compensated for by adjustments in $\psi(t)$ in the adjacent intervals. This indicates that our actual time resolution is poorer than the 3 Gyr interval we have used; i.e., we can reproduce the observations for example, having many stars older than 12 Gyr and a few between 9 and 12 Gyr or vice versa. Nevertheless, coupling seems stronger between intervals from 15 to 9 Gyr and between intervals from 9 to 1 Gyr. For this reason we have averaged $\psi(t)$ in these wider intervals. The resulting function is much better constrained. This can be seen in Fig. 10, which shows that:

•For $d=0.77$ Mpc, $\psi(t)$ must not have been very different from constant from 15 to 1 Gyr ago and it has decreased by a factor of ~ 3 in the last 1 Gyr. The estimate by Mould (1997) of a decreasing of $\psi(t)$ by a factor 10 seems too large in the light of our models.

•For $d=0.96$ Mpc, $\psi(t)$ decreases by factors of ~ 2 between the periods running from 15 to 9 Gyr, from 9 to 1 Gyr and from 1 to 0 Gyr. Defining $\tau=15-t$, $\psi(\tau)$ can be fitted by an exponential law of the form

$$\psi(\tau)=\psi_0 e^{-\tau/\beta}$$

with $\psi_0=1.5\times10^{-4}$ $M_\odot$ yr^{-1} and $\beta=7.1$ Gyr.

We have seen that time resolution in the interval from 15 to 9 Gyr is poor, so that we hardly could say anything about the precise time of the beginning of the star formation in LGS 3. The fact that 100% of the accepted models have star formation in that interval is a strong indication of an early

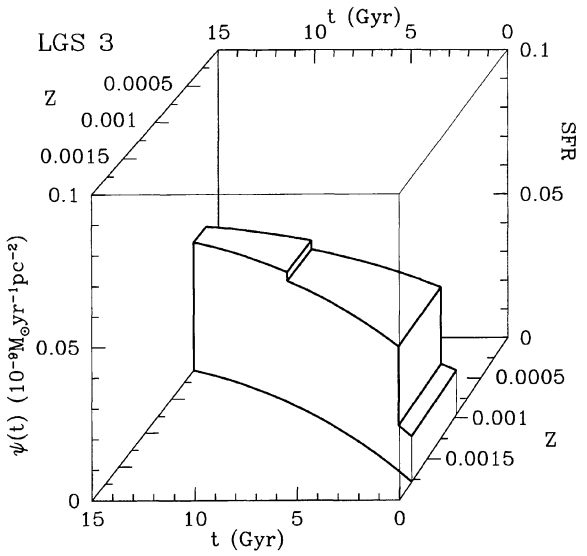

FIG. 11. The population box of LGS 3 represents the SFH of the galaxy combining the two key functions: $\psi(t)$ and $Z(t)$. Results for distance $d=0.77$ Mpc have been used because this seems the most likely distance for the galaxy.

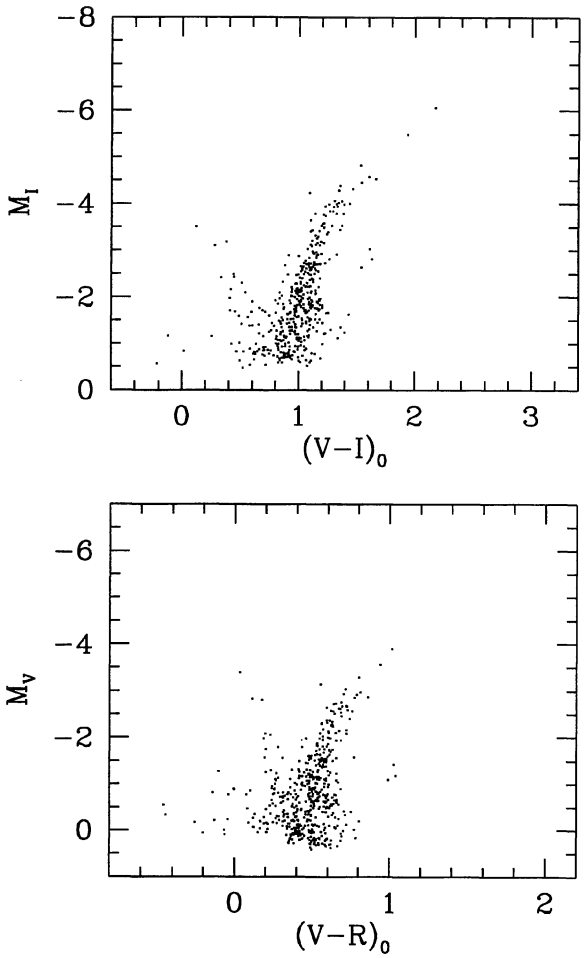

FIG. 12. Model CM diagrams produced by the SFH shown in Fig. 11. They are the ones better reproducing observations (Figs. 3 and 4).

epoch for the beginning of the star formation, reinforced by the fact that 97% of the accepted models have star formation from 15 Gyr ago. Note for comparison that 90% of the computed models have star formation since 15 Gyr ago. These figures are valid for both distances.

A similar question can be raised about $\psi(t)$ at present date. The fact that LGS 3 has no H II regions could indicate that $\psi(0)=0$. But the values found for the last 1 Gyr ($(1.5\pm0.1)\times10^{-5}$ $M_\odot$ yr^{-1} for $d=0.77$ Mpc and $(1.9\pm0.3)\times10^{-5}$ $M_\odot$ yr^{-1} for $d=0.96$ Mpc) combined with the IMF by Kroupa *et al.* (1993), results in a probability of LGS 3 having a star massive enough to produce an H II region of about 0.2, compatible with observations.

Figure 11 shows the population box (see Hodge 1989) for LGS 3 plotted using the results of distance 0.77 Mpc. The figure simultaneously shows $\psi(t)$ and $Z(t)$ and is a global representation of the SFH of the galaxy. Figure 12 shows the model CM diagrams produced by the SFH plotted in Fig. 11. These diagrams can be considered the ones better reproducing the observed diagrams shown in Figs. 3 and 4.

Figure 13 shows a model CM diagram produced by the SFH plotted in Fig. 11 also, but simulating the observational effects expected if the limiting magnitude were ~3 mag deeper than in our data. This is what would be obtained from deep *HST* observations, if our conclusions are correct. Note that the well developed HB is produced by the presence of a significant amount of very old, low metallicity stars in the adopted model. Eventual differences in the observed HB would imply a different SFH for the first ~1 Gyr. It is in fact the morphology of the HB which would provide details on the SFH for that very early period. Similarly, the distribution of MS stars will provide details about the SFH in the last ~1 Gyr.

7. THE CHEMICAL ENRICHMENT SCENARIO

We have calculated $\psi(t)$ and $Z(t)$ laws that reproduce the CM diagram of LGS 3. Now we will investigate what chemical evolutionary scenarios make compatible the $\psi(t)$ and $Z(t)$ found, i.e., under what overall conditions $\psi(t)$ as shown in Fig. 10 produce $Z(t)$ as shown in Fig. 5. For each distance, we have computed the $Z(t)$ that would be produced by our $\psi(t)$ for a simple closed box scenario and for families of infall and outflow scenarios. Following Peimbert *et al.* (1994, and references therein) we assume the infall rate as given by $f_I=\alpha(1-R)\psi$ and the outflow of well mixed material by $f_O=\lambda(1-R)\psi$, where R is the returned fraction (Tinsley 1980) and α and λ are parameters. Outflow of non mixed Z-rich material has been also considered and is characterized by the parameter γ, defined as the fraction of freshly made metals that are ejected to the intergalactic medium without mixing with the interstellar gas. A returned fraction $R=0.2$, accordingly to our stellar evolutionary models, and a gas fraction $\mu=0.4$ have been used (see Sec. 8 and Table 3). Figure 14 shows a number of the chemical enrichment laws we have computed in this way, overimposed to the $Z(t)$ laws found for LGS 3 shown in Fig. 5.

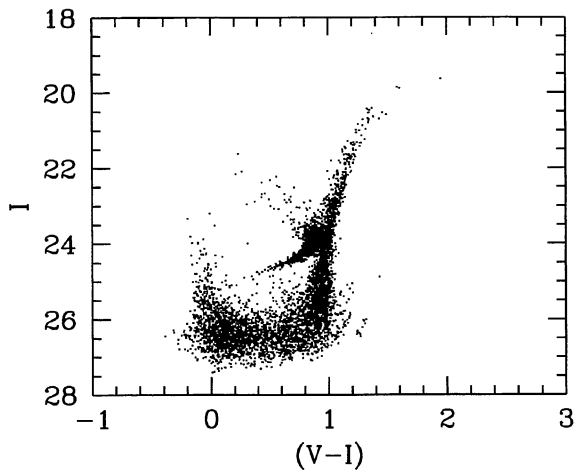

FIG. 13. Model CM diagram produced by the SFH shown in Fig. 11 simulating the observational effects expected if the limiting magnitude were ~3 mag deeper than in this paper. This is what would be seen from deep *HST* observations if our conlusions for the SFH are correct.

In the case of $d=0.77$ Mpc, a closed box produces a $Z(t)$ law not very different to that we have found for LGS 3, but a better fit is obtained with a moderate outflow of well mixed material given by $\lambda=3$. In contrast, large rates of infall or outflow would produce $Z(t)$ increasing too fast and too slowly, respectively, in the beginning of the galaxy history. The effective yield obtained for the $\lambda=3$ scenario is $y=0.002$ (it is $y=0.0011$ in the closed box case), 7 times smaller than the theoretical value $y=0.014$ found by Peimbert *et al.* (1994) using models by Maeder (1992) for a system with $Z=0.001$. Effective and theoretical yields can be reconciled if, in addition, outflow of Z-rich material at a rate $\gamma=0.85$ is allowed. Since the material escaping from the galaxy without mixing would mostly be that coming from SN explosions, this would modify the rates of chemical elements present in the interstellar medium and successive generations of stars. In particular, following the results by Peimber *et al.* (1994, and references therein) the ratio $\Delta Y/\Delta Z(O)$ would be 4 times larger than if no outflow of Z-rich material would exist. This value is not far from the factor 2.4 (which corresponds to $\gamma=0.73$) found by Peimbert *et al.* (1994) for a sample of irregular and blue compact galaxies (see also Pagel *et al.* 1992).

In the case of $d=0.96$ Mpc, a large outflow of well mixed material at a rate $\lambda\simeq 30$ is required to reconcile the $\psi(t)$ and $Z(t)$ functions of LGS 3 (see Fig. 14). The effective yield is now $y=0.009$. Additional outflow of Z-rich material at a rate $\gamma=0.36$ would reconcile this yield with the theoretical one.

8. INTEGRATED PROPERTIES OF LGS 3

The results found for $\psi(t)$ can be used to calculate integrated properties. The most relevant ones are summarized in Table 3 for both distances. $\bar{\psi}$ is the average of $\psi(t)$ from 15 Gyr ago to date. We cover in our observations almost the full optical body of the galaxy, but not completely. In this sense,

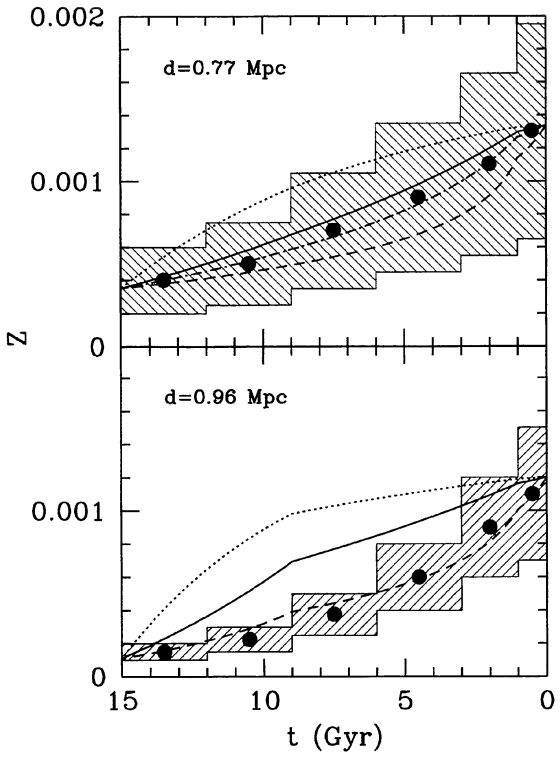

FIG. 14. Chemical enrichment laws for different scenarios produced by the $\psi(t)$ functions shown in Fig. 10 superimposed to the $Z(t)$ laws found for LGS 3. In both panels, dots mark the centers of the $Z(t)$-t boxes. Full lines correspond to a closed box scenario; dotted lines to an infall scenario in which infall is balanced by star formation ($\alpha=1$) and dashed lines to an outflow scenario in which outflow is 30 times the mass locked into stars and stellar remnants ($\lambda=30$). In the upper panel, the dot-dashed line corresponds to an outflow scenario with $\lambda=3$.

the actual value of $\bar{\psi}$ should be slightly larger than that given in the table. The value of $\bar{\psi}$ normalized to the observed area is also given ($\bar{\psi}/A$). $\bar{\psi}_{1\,\mathrm{Gyr}}$ is the average value of $\psi(t)$ for the last 1 Gyr and is also given per unit area ($\bar{\psi}_{1\,\mathrm{Gyr}}/A$). $Z(0)$ is the current metallicity. $M_\star$ is the mass locked into stars and stellar remnants obtained from integration of $\psi(t)$ and using the IMF of Kroupa *et al.* (1993). M_{gas} and M_{tot} have been calculated using the results by Lo *et al.* (1993) and assuming the gas mass to be 4/3 of the H I mass. To compute the B luminosity, L_B, the apparent magnitude $B_T=16.18$ by Karachentseva *et al.* (1996) has been used. For the galactic extinction we have used $A_{Bg}=0.16$ (see Sec. 4) and we have computed the internal extinction as $A_{Bi}=0.75\log R$ (de Vaucouleurs *et al.* 1991), where $R=1/0.67$ for LGS 3 (Karachentseva *et al.* 1996). For the solar absolute magnitude, $M_{B\odot}=5.54$ has been used, after Durrant (1981). μ is the fraction of gas relative to the total mass intervening in the chemical evolution: $\mu=M_{\mathrm{gas}}/(M_\star+M_{\mathrm{gas}})$. As dark matter, we consider the mass that cannot be explained as stellar remnants or by extrapolation of the Kroupa *et al.* (1993) IMF to low masses. The fraction of dark matter is computed as $1-(M_\star+M_{\mathrm{gas}})/M_{\mathrm{tot}}$. $M_{\mathrm{b},0}$ is the initial mass intervening in the chemical evolution. It is computed as the current value of $M_\star+M_{\mathrm{gas}}$ corrected of the outflow found in Sec. 7. This

TABLE 3. Global properties of LGS 3.

		$d=0.77$	$d=0.96$
$\bar{\psi}$	($M_\odot yr^{-1}$)	$(4.0\pm0.4)\times10^{-5}$	$(5.9\pm0.4)\times10^{-5}$
$\bar{\psi}/A$	($M_\odot yr^{-1}pc^{-2}$)	$(1.4\pm0.1)\times10^{-10}$	$(1.4\pm0.1)\times10^{-10}$
$\bar{\psi}_{1Gyr}$	($M_\odot yr^{-1}$)	$(1.5\pm0.1)\times10^{-5}$	$(1.9\pm0.3)\times10^{-5}$
$\bar{\psi}_{1Gyr}/A$	($M_\odot yr^{-1}pc^{-2}$)	$(0.55\pm0.04)\times10^{-10}$	$(0.47\pm0.07)\times10^{-10}$
$Z(0)$		0.0007–0.002	0.0007–0.0015
$M_\star$	($M_\odot$)	4.8×10^5	6.4×10^5
M_{gas}	($M_\odot$)	$(3.2\pm0.4)\times10^5$	$(4.7\pm0.6)\times10^5$
M_{tot}	($M_\odot$)	$(1.8\pm1.0)\times10^7$	$(2.2\pm1.2)\times10^7$
L_B	($L_\odot$)	4.3×10^5	6.4×10^5
$\mu=M_{gas}/(M_\star+M_{gas})$		0.40	0.40
Dark matter		95%	95%
$M_{b,0}$	($M_\odot$)	2.3×10^6	2.0×10^7
M_{gas}/L_B	($M_\odot/L_\odot$)	0.74	0.74
M_{tot}/L_B	($M_\odot/L_\odot$)	41	34
Distance to M33	(Mpc)	0.18	0.22
Distance to M31	(Mpc)	0.25	0.34
Distance to LG	(Mpc)	0.37	0.55

outflow is $(\lambda+\gamma R/(1-R))M_\star$, where we have used $R=0.2$, according to ours models. In the case $d=0.77$ Mpc, $\lambda=3$ and $\gamma=0.85$. In the case $d=0.96$ Mpc, $\lambda=30$ and $\gamma=0.36$. Note that the value $M_{b,0}=2.0\times10^7$ $M_\odot$ obtained for $d=0.96$ Mpc is close to the dark matter mass (2.1×10^7 $M_\odot$), indicating that, if this mass is constant in the galaxy, its amount could have been about 50% of the total initial mass of the galaxy.

The next two lines of Table 3 give the gas and total mass-luminosity relation. The last three lines contain the distances of LGS 3 to M33, to M31 and to the barycenter of the LG. To calculate this, we have used the distance from the Milky Way to M33 and M31 to be, respectively, 0.84 Mpc (Freedman *et al.* 1991) and 0.77 Mpc (Freedman & Madore 1990) and the barycenter of the LG to be situated in the line connecting M31 and the Milky Way, at a distance of 0.45 Mpc from the Milky Way. This results from adopting, after Peebles (1989), a mass for the Milky Way 0.7 times that of M31 and neglecting the masses of any other galaxy in the LG.

Let us go back to the idea that LGS 3 might be a dIr-dE intermediate-type galaxy. As we have mentioned, indications for this are that the galaxy shows a small amount of gas but neither H II regions nor a well populated MS. However, we have seen that LGS 3 shows an M_{gas}/L_B ratio close to 1 and that its CM diagram is compatible with a roughly constant star formation starting 15 Gyr ago and with a present rate not much lower than its average for the past. Furthermore, LGS 3 has enough gas to be forming stars for some 30 Gyr more from now at the present rate or for some 10 Gyr more from now at the averaged rate $\bar{\psi}$. All this would not be surprising for a dIr. The characteristic of LGS 3 which makes it different from other dIrs are its absolute parameters. M_{tot}, M_{gas}, $M_\star$, L_B, and $\bar{\psi}$ are one or two orders of magnitude smaller that those for typical dIr galaxies. As a result, we conclude that LGS 3 does not show any H II region for reasons of simple probability and not necessarily because it is in a quiescent phase of its star formation. In summary, LGS 3 might well be a dIr just on the tail of the mass, luminosity and SFR distributions.

9. CONCLUSIONS

Photometry in the V, R, and I Johnson-Cousins bands of 736 stars resolved in LGS 3 is presented. The galaxy shows CM diagrams where the main feature is a narrow red-tangle, but very few red-tail or blue stars are present. The distance of the galaxy is estimated using the luminosity of the TRGB. A splitting of the upper part of the RGB prevents a unique determination and forces the assumption of two possible values for the distance: $d=0.77\pm0.07$ Mpc and $d=0.96\pm0.07$ Mpc. From the analysis of the SFH, indications that 0.77 ± 0.07 is the best estimate are obtained.

The SFH of the galaxy is investigated. We consider the SFH as the combination of two time-dependent functions: the SFR $\psi(t)$ and the CEL $Z(t)$, the IMF being assumed as a fixed input. The SFH has been studied through the comparison of the observed CM diagrams with model CM diagrams which result from different choices of $\psi(t)$ and $Z(t)$. The following approach has been used: first, the numbers of stars produced by a small number of simple-shaped star formation rates $\psi(t)$ (we call them ψ_i) are computed in several regions of the CM diagram. Each ψ_i produces stars at a constant rate for a short interval of time, and in a given metallicity interval. The distribution of stars in the CM diagram produced by an arbitrary $\psi(t)$ is then computed as a linear combination of the results for the ψ_i functions, as explained in Sec. 5. We call each of these linear combinations a *global model*. In total, 10^6 global models have been calculated. We have selected all those that reproduce the numbers of stars in previously defined regions of the observed CM diagrams better than 1.33σ for $d=0.77$ Mpc and 2σ for $d=0.96$ Mpc. 2.5% of the models fulfill each condition.

The $\psi(t)$ functions resulting from average of all the accepted models are represented in Figs. 10 and 11. The results can be summarized as follows:

•For both possible distances star formation beginning 15 Gyr or, at least, 12 Gyr ago is favored. Nothing can be said about short time bursts in the past, since the CM of LGS 3 does not give enough resolution for ages older than 1 Gyr.

•An almost constant function from 15 to 1 Gyr ago and stepping down by a factor ~ 3 since 1 Gyr ago (in the case of $d=0.77$ Mpc) or an exponentially decreasing function with $\beta=7.1$ Gyr extending from 15 Gyr ago to date (in the case of $d=0.96$ Mpc) are likely shapes for $\psi(t)$.

•The average value of $\psi(t)$ for the entire lifetime of the galaxy is $\bar{\psi}=(1.4\pm 0.1)\times 10^{-10}$ $M_\odot$ yr^{-1} pc^{-2} for both distances.

•The current metallicity ranges from $Z\simeq 0.0007$ to $Z\simeq 0.002$ for $d=0.77$ Mpc and from $Z\simeq 0.0007$ to $Z\simeq 0.0015$ for $d=0.96$ Mpc.

•Using $\bar{\psi}_{1\ \mathrm{Gyr}}$ as a good representation of the present SFR, the probability of LGS 3 having an H II region is about 0.2, compatible with the observation of no H II regions in the galaxy.

•The gas fraction of LGS 3 relative to the mass intervening in the chemical evolution is about 0.4.

•About 95% of the mass of LGS 3 is dark matter, i.e., mass that is neither explained by stellar remnants nor by an extrapolation of the Kroupa *et al.* (1993) IMF to low-mass stars.

•Outflow of well mixed material is required to make compatible the $\psi(t)$ and $Z(t)$ found. For the case of $d=0.77$ Mpc, a relatively moderate outflow given by $\lambda=3$ is enough, but $\lambda\simeq 30$ is required for the case $d=0.96$ Mpc. Effective yields are smaller than theoretical ones derived from stellar evolution models of Maeder (1992). Outflow of a fraction $\gamma=0.85$ of non mixed, freshly made metals, in the case $d=0.77$ Mpc, and of $\gamma=0.36$ in the case $d=0.96$ Mpc, would account for the differences between effective and theoretical yields.

•The large outflow rate $\lambda\simeq 30$ required in the case $d=0.96$ Mpc would imply that most of the initial gas of the galaxy has been lost and that the initial dark matter fraction would have been as low as $\sim 50\%$.

•The M_{gas}/L_B ratio is 0.74, similar to what is common in dIr galaxies. With the observed M_{gas}, LGS 3 can continue to form stars for some 30 Gyr more at the present rate or for some 10 Gyr more at a rate equal to $\bar{\psi}$.

•The distances of LGS 3 to M33 and M31 are respectively 0.18 and 0.25 Mpc if $d=0.77$ Mpc, or 0.22 and 0.34 Mpc if $d=0.96$ Mpc.

In summary, LGS 3 shows characteristics of typical dIrs (gas fraction, M_{gas}/L_B rate, behaviour of $\psi(t)$), the main differences being that its mass, luminosity and SFR (present and averaged) are one to two orders of magnitude too small. This makes the absence of H II regions a simple probabilistic effect. Taking into account all the properties of LGS 3, it may be considered a dIr just on the tail of the distributions of mass, luminosity and SFR, and not necessarily a dIr-dE transition object.

We are indebeted to Cesare Chiosi for his permanent contribution to the development of this project and for many fruitful discussions concerning this particular paper. We thank Leo Girardi and Paola Marigo for their contributions to the implèmentation of the mass loss algorithm in the synthetic diagrams code. We also thank Wendy Freedman for many interesting comments. This work has been substantially improved after fruitful suggestions made by an anonymous referee. This work has been financially supported by the Instituto de Astrofísica de Canarias (grant P3/94) and by the Dirección General de Investigación Científica y Técnica of the Kingdom of Spain (grant PB94-0433).

REFERENCES

Aparicio, A., & Gallart, C. 1994, in The Local Group: Comparative and Global Properties, ESO Conference and Workshop Proceedings No. 51, edited by A. Layden, R. C. Smith, and J. Storm (ESO, Garching), p. 115
Aparicio, A., & Gallart, C. 1993, Noticias del IAC, N. 4-1993, 7
Aparicio, A., & Gallart, C. 1995, AJ, 110, 2105
Aparicio, A., Gallart, C., & Bertelli, G. 1997, AJ, (in press)
Baade, W. 1963, in The Evolution of Stars and Galaxies, edited by C. Payne-Gapsochkin (Harvard University Press, Harvard)
Bertelli, G., Bressan, A., Chiosi, C., Fagotto, F., & Nasi, E. 1994, A&AS, 106, 271
Bürstein, D., & Heiles, C. 1984, ApJS, 54, 33
Christian, C., & Tully, R. B. 1983, AJ, 88, 934
Da Costa, G. S. 1997, in Stellar Astrophysics for the Local group, edited by A. Aparicio, A. Herrero, and F. Sánchez (Cambridge University Press, Cambridge) (in press)
Da Costa, G. S., & Armandroff, T. E. 1990, AJ, 100, 162
de Vaucouleurs, G., de Vaucouleurs, A., Corwin, H. G., Buta, R. J., Paturel, G., & Fouqué, P. 1991, Third Reference Catalog of Bright Galaxies (Springer, New York)
Durrant, C. J. 1981, in Landolt-Börnstein New Series, edited by K.-H. Hellwege, Group VI, K. Schaifers, and H. H. Voigt (Springer, Berlin), Vol. 2a, p. 82
Freedman, W. L. 1994, in The Local Group: Comparative and Global Properties, ESO Conference and Workshop Proceedings No. 51, edited by A. Layden, R. C. Smith, and J. Storm (ESO, Garching), p. 227
Freedman, W. L., & Madore, B. F. 1990, ApJ, 365, 186
Freedman, W. L., Wilson, C. D., & Madore, B. F. 1991, ApJ, 372, 455
Gallagher, J. S., & Wyse, R. F. G. 1994, PASP, 106, 1225
Gallart, C., Aparicio, A., Bertelli, G., & Chiosi, C. 1996b, AJ, 112, 1950
Gallart, C., Aparicio, A., Bertelli, G., & Chiosi, C. 1996c, AJ, 112, 2596
Gallart, C., Aparicio, A., & Vílchez, J. M. 1996a, AJ, 112, 1928
Hodge, P. 1989, ARA&A, 27, 139
Karachentseva, V. E. 1976, Comm. Special Obs., 18, 42
Karachentseva, V. E., Prugniel, Ph., Vennink, J., Richter, G., Thuan, T., & Martin, J. 1996, A&AS, 117, 343
Kroupa, P., Tout, C. A., & Gilmore, G. 1993, MNRAS, 262, 545
Landolt, A. U. 1992, AJ, 104, 340
Lee, M. G. 1995, AJ, 110, 1129
Lee, M. G., Freedman, W. L., & Madore, B. F. 1993, ApJ, 417, 553
Lo, K. Y., Sargent, W. L. W., & Young, K. 1993, AJ, 106, 507
Maeder, A. 1992, A&A, 264, 105
Majewski, S. R. 1994, ApJ, 431, L17
Mould, J. 1997, PASP, 109, 125
Pagel, B. E. J., Simonson, E. A., Terlevich, R. J., & Edmunds, M. G. 1992, MNRAS, 255, 325
Peebles, P. J. E. 1989, ApJ, 344, L53
Peimbert, M., Colín, P., & Sarmiento, A. 1994, in Violent Star Formation,

edited by G. Tenorio-Tagle (Cambridge University Press, Cambridge), p. 79
Schild, R. 1980, ApJ, 242, 63
Smecker-Hane, T. A., Stetson, P. B., Hesser, J. E., & VandenBerg, D. A 1996, in From Stars to Galaxies: The Impact of Stellar Physics on Galaxy Evolution, ASP Conf. Ser. 98, edited by C. Leitherer, U. Fritze-von Alvensleben, and J. Huchra (ASP, San Francisco), p. 328
Stetson, P. B. 1993, User's Manual for DAOPHOT II
Stetson, P. B., & Harris, W. E. 1988, AJ, 96, 909
Thuan, T. X., & Martin, G. E. 1979, ApJ, 232, L11
Tifft, W. G., & Cocke, W. J. 1988, ApJS, 67, 1
Tikhonov, N., & Makarova, L. 1996, AJ, 317, 179
Tinsley, B. M. 1980, Fundam. Cosm. Phys., 5, 287
Van de Rydt, F., Demers, S., & Kunkel, W. E. 1991, AJ, 102, 130